Physical model of deformation and rupture of blood vessels in the human cardiovascular system

Maxwell Cole
Louisiana State University
Wayne Newhauser
Louisiana State University
Patrick Diehl
diehlpk@lanl.gov

Louisiana State University
Pablo Seleson
Oak Ridge National Laboratory

Research Article

Keywords: vascular modeling, rupture, peridynamics, biophysical modeling

Posted Date: June 12th, 2026

DOI: https://doi.org/10.21203/rs.3.rs-9728551/v1

Additional Declarations: No competing interests reported.

Physical model of deformation and rupture of blood vessels in the human cardiovascular system

Maxwell Cole[1*], Wayne Newhauser[1,2], Patrick Diehl[1,3,4], Pablo Seleson[5]

[1]Department of Physics & Astronomy, Medical and Health Physics Program, Louisiana State University, Nicholson Hall Baton Rouge, LA 70802, USA.
[2]Mary Bird Perkins Cancer Center, 4950 Essen Lane Baton Rouge, LA 70809, USA.
[3]Center for Computation & Technology, Louisiana State University, 888 S Stadium Dr Baton Rouge, LA 70808, USA.
[4]Computing and Artificial Intelligence Group, Los Alamos National Laboratory, Mail Stop B287, Los Alamos, NM 87544, USA.
[5]Computer Science and Mathematics Division, Oak Ridge National Laboratory, P.O. Box 2008, MS-6013, Oak Ridge, TN 37831-6013, USA.

*Corresponding author(s). E-mail(s): m6cole@health.ucsd.edu;
Contributing authors: newhauser@lsu.edu; diehlpk@lanl.gov;
selesonpd@ornl.gov;

Abstract

Cardiovascular diseases often originate from localized vascular failures that escalate to systemic complications. Modeling these failures, particularly vessel rupture, is critical for early diagnosis and treatment planning. This study presents a computational model of blood vessel deformation and rupture based on peridynamics (PD), a non-local theory of solid mechanics that overcomes limitations of classical continuum mechanics in handling discontinuities. We developed a PD-based model of a single blood vessel, entitled PeriVessel, to simulate blood-pressure-induced vascular rupture. The PeriVessel model was then integrated with a prototype whole-body cardiovascular digital twin (CVDT) representing approximately 34 billion vessels. The coupled PD-CVDT model was evaluated

for computational feasibility by measuring execution time, floating-point operations, and memory usage across various scales. Results demonstrated that PD could accurately model vessel rupture progression, with initiation observed at physiological pressures consistent with experimental data. The integration of the PeriVessel model with the Base CVDT required an increase in computational resources of less than 2%, indicating strong scalability and feasibility. This represents the first demonstration of simulating vessel rupture within a prototype full-body CVDT, laying the groundwork for future predictive modeling in clinical applications such as stroke risk assessment. The study underscores the viability of combining high-fidelity biomechanical models with large-scale vascular simulations, advancing the realism and utility of digital twin technologies in cardiovascular research.

Keywords: vascular modeling, rupture, peridynamics, biophysical modeling

1 Introduction

Systemic changes in large physical systems can initiate localized failures at the microscopic scale, particularly in networks governed by complex physical phenomena. These microscopic failures can, subsequently, lead to further deleterious effects at the macroscopic scale [1]. Multiscale cascades of failures are especially relevant in the natural history of cardiovascular diseases (CVDs). CVDs encompass many conditions affecting the heart and blood vessels, which together comprise the leading cause of morbidity and mortality worldwide [2]. A precursor to many systemic CVDs is the onset of localized microscopic changes to blood vessels. Among vascular conditions with significant multiscale effects, cerebral aneurysms are particularly dangerous. Aneurysms typically arise from changes in blood flow that increase mechanical forces, such as hypertension, progressively weakening the vessel wall [3]. As structural integrity deteriorates, histological changes further disrupt hemodynamic stability, impairing the vessel's ability to maintain homeostasis. This leads to increased blood pressure and continued dilatation, which, if left untreated, can progress to rupture. The consequences of vessel rupture are severe, including vascular dysfunction, chronic neurodegenerative disorders, stroke, or even death [4, 5].

The ability to model and predict blood vessel rupture would be helpful for early diagnosis, risk assessment, and treatment planning [6]. By understanding how localized vascular failures propagate into systemic consequences, researchers can develop more effective prevention and intervention strategies. Computational modeling has proven to be a powerful tool for simulating the biomechanical behavior of blood vessels [7]. Together with the emergence of cardiovascular digital twin (CVDT) technologies, biomathematical modeling has the potential to offer insights into vascular health under various physiological conditions [8]. CVDTs are virtual representations of the entire human circulatory system that, in theory, could provide real-time simulation and predictive analytics [9]. Incorporating rupture mechanics into CVDTs will become

essential for personalized cardiovascular risk modeling but presents a challenging set of computational problems [10].

The mechanical properties of blood vessels are well-understood from engineering and biomedical research. Modeling of vessel deformation usually utilizes continuum mechanics methodologies [11]. Classical continuum mechanics (CCM) is a mathematical formulation governing mechanical forces in deformable materials [12], in which a material is modeled as a continuous medium, as opposed to a set of discrete particles. Continuum-based blood vessel constitutive relations have been effectively used in biomechanical modeling applications, with the finite element method (FEM) being a common numerical modeling approach. FEM divides a continuous medium into smaller elements, typically employing mesh-based methods, to approximate solutions to differential equations [13]. Several research groups, such as Raghavan and Vorp [14] and Seshaiyer and Humphrey [15], have used FEM to model aneurysm mechanics. However, if vessel rupture is considered in the simulation, CCM methods can fail when dealing with discontinuous features, such as a fracture [16, 17]. This is because these methods rely on the use of spatial derivatives in the governing equations, which are undefined at discontinuities, e.g., microscopic defects that can nucleate fractures.

Fracture mechanics is a well-established field of research concerned with material failure [18]. FEM and a variety of related methods have been used to model material failure and the propagation of cracks in solid media [19]. To circumvent issues with discontinuities or singularities, these methods typically begin with a preexisting initial tear at a predicted failure site [20, 21]. However, CCM methods often struggle to predict tear initiation or the locations where cracks originate. An alternative approach, called peridynamics (PD), was introduced by Silling in 2000 [16]. PD is a non-local extension of CCM that is based on integro-differential governing equations, making it especially well-suited for modeling fracture since it avoids the need for spatial derivatives. Bond-based PD [16] represents material deformation through pairwise

forces that operate via bonds. Later, state-based PD was developed [22], in which material deformation is represented through force states. The field has grown rapidly since its inception [23] and has been applied to a multitude of fracture simulations. In the context of biomechanical modeling, PD has proven to be capable of modeling cortical bone fracture [24], biomembrane rupture [25], as well as tumor growth [26] and shrinkage [27].

Compared to CCM methods, PD requires increased memory usage and computational resources due to its non-local interactions, leading to a higher number of floating-point (FP) operations per time step [28, 29]. Recently, parallel computing and GPU acceleration have been implemented in PD simulations to improve scalability [30]. However, integrating PD into large-scale vascular models, such as the whole-body CVDT previously reported by our laboratory [9], introduces additional challenges related to increased execution time and handling of large amounts of data. While the feasibility of a simplistic CVDT has been demonstrated, the coupling of PD vessel damage simulations with a full-body vascular network is unexplored. A critical question is whether PD can be feasibly integrated within a CVDT framework with currently available computational resources.

This study aims to evaluate the feasibility of adapting PD to predict the origination and propagation of blood vessel fracture damage. To this end, we developed a bond-based PD model of blood-pressure-induced vessel deformation and rupture called PeriVessel. We assessed the PeriVessel model's computational performance by measuring metrics, such as execution time, number of FP operations, and memory usage. We then coupled this model with our CVDT model and characterized the integrated PD-CVDT model's computational requirements and scalability. The study employs the PD theory for fracture modeling and leverages high-performance computing (HPC) techniques to optimize execution time. By analyzing the trade-offs between accuracy, computational complexity, and integration feasibility, this research provides insights

into the potential for analyses of vascular damage and failure mechanics in digital twin applications.

The principal innovation of this study lies in the development and incorporation of a PD vessel model within our established CVDT framework. This coupling enables the analysis of vascular damage and rupture within a whole-body system, which has not been previously achieved in existing models. This paper is organized as follows. We first present the results of the simulations in Section 2. In Section 3, we give an overview of the methods, including the PD framework in Section 3.1, the PeriVessel model and coupled PD-CVDT model in Sections 3.2 and 3.3, respectively, and a description of the computational implementation and metrics for testing the performance in Section 3.4. Finally, in Section 4, we provide conclusions and discuss future directions of this line of work.

2 Results

In the PeriVessel simulation, the prescribed net pressure of 238 kPa ruptured the vessel wall, as expected. The vessel exhibited a transmural rupture consistent with high intraluminal pressure leading to outward extension and eventual rupture [31]. Figure 1 displays the simulation results at selected time points. The left column shows the vessel with colors representing the computational particle's displacement magnitude relative to the reference configuration. The colors in the right column represent the particle's damage (described in (6)). The effect of the pressure is seen beginning at 1.85 ms, causing radial expansion of the vessel wall with a maximum displacement magnitude of approximately 0.5 mm. At this time, we also observe the initiation of the rupture at the midline of the vessel, with particles exhibiting damage ranging from 20% to 30%. The rupture progressed from the vessel lumen to the superficial wall and began propagating longitudinally in both directions until reaching a length of approximately

8 mm. At 2.25 ms, the particles on the edge of the rupture have a maximum damage of 47%, with maximal vessel wall displacement magnitude of 2 mm.

The computational complexity and required resource usage, $R(p)$, of our models are plotted in Figure 2 along with the empirical fits using (10), with parameters listed in Table 1. The computational resource usage for each model is governed by the problem size, p. The Base CVDT and PD-CVDT models scaled in proportion to the number of vessels in the vascular network, i.e., $p = N_V$ in (10). However, $N_V = 1$ for the PeriVessel model. We, therefore, characterize the resource usage in the PeriVessel model in terms of the number of compute nodes, i.e., $p = N_c$. The graphs display the execution node-time, R_T, number of FP operations, R_{FP}, and maximum memory usage, R_M, in Figure 2(a), (b), and (c), respectively.

All models showed computational feasibility across the entire range of compute nodes and network sizes considered. The Base CVDT model exhibited computational complexity, and required resource usage consistent with previous studies from our laboratory, on the order of $\mathcal{O}(N_V)$ [9, 32]. The PeriVessel simulation was found to have a computational complexity on the order of $\mathcal{O}(N_c)$. This is likely due to the parallel programming ecosystem used by the model, i.e., as the number of compute nodes increased, the amount of inter-node communication also increased. Resource usage for the coupled PD-CVDT simulations was dominated by the Base CVDT model, also exhibiting a computational complexity on the order of $\mathcal{O}(N_V)$.

For the PeriVessel model, the execution wall-clock time ranged from 384 s on one compute node with 48 cores to 5.9 s on 1024 compute nodes with a total of 49,152 cores. This corresponded to a node-time of 0.11 and 1.68 node-hours, respectively. The simulation required 1.27×10^{12} FP operations, which remained approximately constant for the range of compute nodes used. However, the maximum memory usage of the simulation increased as the number of compute nodes increased, ranging from 0.89 GB on one compute node to 165.8 GB on 1024 compute nodes. We believe this increase

Table 1 Fitted parameters from (10) to the required resources, R, for each model. The problem size, p, corresponds to the parameter that drives resource usage for each model: the number of vessels, N_V, for the Base CVDT and PD-CVDT models, or the number of compute nodes, N_c, for the PeriVessel model.

R	α	β	p	γ
PeriVessel Time	0.106	1.54×10^{-3}	N_c	1.0
PeriVessel FP	1.27×10^{12}	0.0	N_c	-
PeriVessel Memory	0.71	0.18	N_c	0.98
Base CVDT Time	0.0	1.47×10^{-9}	N_V	1.05
Base CVDT FP	0.0	1.21×10^{6}	N_V	0.58
Base CVDT Memory	0.0	8.14×10^{-7}	N_V	1.0
Coupled PD-CVDT Time	0.0	1.59×10^{-9}	N_V	1.04
Coupled PD-CVDT FP	1.27×10^{12}	1.21×10^{6}	N_V	0.58
Coupled PD-CVDT Memory	0.0	8.22×10^{-7}	N_V	1.0

in memory was a result of the parallel programming framework, which partitioned particles across compute nodes. Near partition boundaries, each compute node stored duplicates of neighboring nodes' particles to capture nonlocal interactions, causing an increase in total memory usage. The PeriVessel model comprised 54,973 particles.

For the coupled PD-CVDT model, the rate of growth of $R(p)$ was also proportional to N_V. The entire body simulation, with 34 billion vessels, required 9.2 minutes of wall-clock time on 1024 compute nodes, corresponding to 157 node-hours. The maximum memory usage, M, closely followed that of the Base CVDT model, ranging from 24.7 GB for 33 million vessels on one compute node to 29 TB for 34 billion vessels on 1024 compute nodes (Figure 2(c)). The total memory usage for the coupled PD-CVDT model was dominated by that of the Base CVDT model. However, the coupled PD-CVDT model required only 0.57% more memory than the Base CVDT model. Similarly, the coupled PD-CVDT model's required node-time, T, was dominated by that of the Base CVDT model, except for smaller network sizes ($N_V \leq 1.35 \times 10^8$), as seen in Figure 2(a). The coupled PD-CVDT simulation of the entire body required only 1.9% more node-hours than the Base CVDT simulation. On the other hand, the required FP operations for the coupled PD-CVDT model were dominated by those

of the PeriVessel model. This is particularly noticeable in Figure 2(b), where the fit using (10) for the coupled PD-CVDT model has a much higher offset than the Base CVDT model due to the PeriVessel model. The coupled PD-CVDT model required 79% more FP operations than the Base CVDT model alone, with a maximum of 2.91×10^{12} FP operations.

The speedup of the PeriVessel model and the parallel efficiency of the Base CVDT model are shown in Figures 2(d) and 2(e), respectively. The PeriVessel model exhibited strong scalability across the range of compute nodes. Figure 2(d) plots the speedup factor, S, versus N_c. The speedup factor, increasing from 1 to 65, sigmoidally approached its theoretical limit of 70, as predicted by strong scaling theory [33, 34]. The Base CVDT model also displayed weak scalability across the range of compute nodes, as displayed in Figure 2(e). The parallel efficiency, ε, ranged from 100% to 46% across the range of vascular network sizes and compute nodes.

3 Methods

3.1 PD framework

Peridynamics (PD) is a non-local continuum mechanics theory [16], and a mesh-free approach [35] is commonly used for large-scale engineering simulations. In this approach, an elastic body is represented by a set of connected computational particles. Each particle i has a reference position $\mathbf{x}_i$ and an associated region of volume V_i, defining the set of reference positions $\{\mathbf{x}_i \in \mathbb{R}^d, i = 1, ..., N\}$ and the set of corresponding particle volumes $\{V_i \in \mathbb{R}, i = 1, ..., N\}$, where N is the total number of particles in the domain and d is the spatial dimension. Here, $d = 3$, as our models are three-dimensional. The particle regions are non-overlapping, and the sum of all particle volumes is approximately equal to the volume of the domain, V (i.e., $\sum_{i=1}^{N} V_i \approx V$) [28]. Each particle i interacts with all other particles within a non-local

neighborhood, $B_\delta(\mathbf{x}_i)$, of radius $\delta > 0$ (this radius is referred to as the horizon), defining a family of interacting particles, $\mathcal{F}_i := \{j \neq i : \|\mathbf{x}_j - \mathbf{x}_i\| \leqslant \delta\}$. The connection between a pair of particles is called a bond.

PD can be considered a continuum analogue of molecular dynamics, which models the movement of atoms or molecules. In PD, however, upon discretization each computational particle represents an aggregation of atoms or molecules, such that the number of PD particles is significantly less than the number of atoms comprising the body, while still being numerous enough to faithfully represent the object's geometry. Similarly, the chemical bonds between atoms or molecules are aggregated into PD bonds. The material and bond aggregations reduce the computational cost of the problem. Leveraging this analogy, the upscaling of molecular dynamics to PD was demonstrated by Seleson et al. [36, 37], resulting in significant computational savings. An illustrative diagram detailing PD particles, bonds, and interactions is displayed in Figure 3.

We used the above-mentioned mesh-free discretization with the prototype microelastic brittle (PMB) constitutive material model developed by Silling and Askari [35]. In the *reference* configuration, or initial undeformed arrangement, particles i and j are located at $\mathbf{x}_i$ and $\mathbf{x}_j$, respectively. The bond between particles i and j is defined as $\boldsymbol{\xi}_{ji} := \mathbf{x}_j - \mathbf{x}_i$. After the body undergoes elastic deformation, particle i is located at position $\mathbf{y}_i$ in the *deformed* configuration, with displacement $\mathbf{u}_i = \mathbf{y}_i - \mathbf{x}_i$. The relative displacement of particles i and j is denoted by $\boldsymbol{\eta}_{ji} := \mathbf{u}_j - \mathbf{u}_i$, and the bond in the deformed configuration becomes $\boldsymbol{\xi}_{ji} + \boldsymbol{\eta}_{ji}$. The discrete PD equation of motion for each particle i is:

$$\rho(\mathbf{x}_i)\ddot{\mathbf{u}}(\mathbf{x}_i, t) = \sum_{j \in \mathcal{F}_i} \mathbf{f}(\mathbf{x}_j, \mathbf{x}_i, t) V_j + \mathbf{b}(\mathbf{x}_i, t), \tag{1}$$

where $\rho(\mathbf{x}_i)$ is the mass density of particle i, $\ddot{\mathbf{u}}(\mathbf{x}_i, t)$ is the acceleration of particle i at time t, $\mathbf{f}(\mathbf{x}_j, \mathbf{x}_i, t)$ is the bond force density (with units of $\mathrm{N/m}^{2d}$) acting on particle i due to particle j at time t, V_j is the volume associated to particle j, and $\mathbf{b}(\mathbf{x}_i, t)$ is a prescribed body force density at particle i at time t [35]. The prescribed body force density, $\mathbf{b}$, represents external forces acting on all particles of the body, as opposed to the internal forces between particles described by the bond force density, $\mathbf{f}$ [16, 38].

The PMB constitutive material model employs the following pairwise bond force density function:

$$\mathbf{f}(\mathbf{x}_j, \mathbf{x}_i, t) = \mu(\mathbf{x}_j, \mathbf{x}_i, t) cs(\boldsymbol{\eta}_{ji}, \boldsymbol{\xi}_{ji}) \frac{\boldsymbol{\xi}_{ji} + \boldsymbol{\eta}_{ji}}{\|\boldsymbol{\xi}_{ji} + \boldsymbol{\eta}_{ji}\|}, \tag{2}$$

where c is the bond elastic constant, s is the bond stretch, and μ is a history-dependent Boolean-valued function that characterizes a bond as intact or broken [35]. An illustration of the bond force density $\mathbf{f}$ given in (2) as a function of the bond stretch s is provided in Figure 4. PD is material agnostic, and the constitutive material model is provided by $\mathbf{f}$. The bond stretch, s, is a unitless scalar equivalent to strain in one dimension, and is defined as:

$$s(\boldsymbol{\eta}_{ji}, \boldsymbol{\xi}_{ji}) := \frac{\|\boldsymbol{\xi}_{ji} + \boldsymbol{\eta}_{ji}\| - \|\boldsymbol{\xi}_{ji}\|}{\|\boldsymbol{\xi}_{ji}\|} = \frac{\|\mathbf{y}_j - \mathbf{y}_i\| - \|\mathbf{x}_j - \mathbf{x}_i\|}{\|\mathbf{x}_j - \mathbf{x}_i\|}. \tag{3}$$

The bond elastic constant characterizes the "stiffness" of the bond and is given by:

$$c = \frac{6E}{\pi\delta^4(1 - 2\nu)}, \tag{4}$$

where E is Young's modulus and ν is Poisson's ratio [35]. Because this constitutive material model is bond-based, $\nu = 1/4$ in 3D [35]. If a bond is stretched beyond its elastic limit, the bond breaks and the force between the particles collapses to zero.

This limit is called the critical stretch and is denoted by s_0. The critical stretch is accounted for in $\mathbf{f}$ through the Boolean-valued function μ, defined as:

$$\mu(\mathbf{x}_j, \mathbf{x}_i, t) := \begin{cases} 1 & \text{if } s(\boldsymbol{\eta}'_{ji}, \boldsymbol{\xi}_{ji}) < s_0 \text{ for all } 0 \leqslant t' \leqslant t, \\ 0 & \text{otherwise,} \end{cases} \tag{5}$$

where $\boldsymbol{\eta}'_{ji}$ is the relative displacement at time t'. The damage at particle i at time t, $\varphi(\mathbf{x}_i, t)$, is quantifiable by the fraction of broken bonds of particle i relative to the total number of its initial bonds in the reference configuration [35]:

$$\varphi(\mathbf{x}_i, t) := 1 - \frac{\sum_{j \in \mathcal{F}_i} \mu(\mathbf{x}_j, \mathbf{x}_i, t) V_j}{\sum_{j \in \mathcal{F}_i} V_j}. \tag{6}$$

A particle with all of its bonds intact has a damage value of 0, whereas a particle with all of its bonds broken has a damaged value of 1.

3.2 PeriVessel model and rupture simulation

We developed a computational model of blood-pressure-driven deformation of a single blood vessel based on the PD theory. For clarity, we refer to this single-vessel PD model as PeriVessel. The PeriVessel model was designed with a general-purpose framework to represent blood vessel deformation and damage as a standalone model or coupled with a large-scale vascular network. To demonstrate this, we created two models: a model of a single vessel under rupture conditions and a model coupled to our laboratory's prototype CVDT model (described in Section 3.3) [9, 39]. Here, we describe the design of the PeriVessel computational model and rupture simulation.

The prescribed body force density, $\mathbf{b}(\mathbf{x}_i, t)$, represents pressures acting on the vessel wall, as shown in Figure 5(a). Under elastic deformation conditions in equilibrium, we

can describe the net pressure, P_{net}, acting on the vessel-blood interface as:

$$P_{\text{net}} = P_{\text{heart}} + P_{\text{g}} - P_{\text{t}} - P_{\text{atm}} - P_{\text{comp}}, \tag{7}$$

where P_{heart} represents the pressure contribution from cardiac output, P_{g} is the pressure from acceleration of the body (e.g., gravity or g-force), P_{t} is the pressure arising from tension in the vessel wall and surrounding tissues, P_{atm} is atmospheric pressure, and P_{comp} is pressure from compressive forces, such as externally worn devices (e.g., tourniquet or g-suit). A diagram illustrating these pressures is shown in Figure 5(b).

The net pressure is a local boundary condition and is applied on the vessel-blood interface at the internal surface of the vessel wall. Because of the non-local nature of PD, local boundary conditions require special considerations [40]. One option is to apply the boundary condition in an extended artificial boundary layer, as proposed by Macek and Silling [41]. This approach has been demonstrated by groups such as Lipton and Jha [42] and Birner et al. [43]. We created this layer of thickness δ, extending inward from the vessel's internal radius, r_0, to apply the force resulting from the pressure (see Figure 5(c)). The body force density was, therefore, calculated by:

$$\mathbf{b}(\mathbf{x}_i, t) = \begin{cases} \frac{1}{\delta} P_{\text{net}} \hat{\mathbf{n}}(\mathbf{x}_i) & \text{if } r_0 - \delta \leqslant r(\mathbf{x}_i) \leqslant r_0, \\ 0 & \text{otherwise,} \end{cases} \tag{8}$$

where $\hat{\mathbf{n}}(\mathbf{x}_i)$ is a unit normal at particle i that points radially outward from the center of the vessel and $r(\mathbf{x}_i)$ is the radial distance of particle i from the center of the vessel.

The standalone blood vessel model was developed to probe the PD simulation under physiological conditions known to cause rupture, thereby providing a benchmark validation case. Therefore, we designed this model to represent a segment of the cerebral artery, with diameter and wall thickness taken from Mandell et al. [44]. The

initial vessel geometry, in the reference configuration, was modeled as a cylinder with a luminal radius of 1.5 mm, an outer radius of 2.0 mm, and a length of 100 mm. We assigned the wall a density of 1.3 g/cm^3 [45] and an elastic modulus of 3.5 MPa [46]. Figure 5(d) illustrates the vessel geometry used in the PD simulation.

The parameters of the simulation are listed in Table 2. We used a particle spacing of $\Delta x = 100$ μm and a horizon of $\delta = 350$ μm. The values of δ and Δx were selected to balance numerical accuracy and computational efficiency [35, 47]. After discretizing the continuous vessel, the total number of particles was $N = 54{,}973$. In the reference configuration, each particle shared bonds with a maximum of 178 other particles. We set the critical stretch value to $s_0 = 0.25$. For time marching, we used explicit time integration with the velocity Verlet scheme [48], using a time step of $\Delta t = 500$ ns. The simulation was run for a total of 4500 time steps, corresponding to a simulation interval of 2.25 ms, to capture damage initiation and rupture propagation in the model under hypertensive vessel-rupture conditions. The pressure required to cause vessel rupture is highly situation-dependent. However, post-mortem experiments by Ciszek et al. [31] found an average rupture pressure of 238 kPa (1785 mmHg) for intracranial arteries. We therefore assigned a net outward pressure of $P_{\text{net}} = 238$ kPa, applied as a uniform load using (8), within the artificial boundary layer adjacent to the vessel-blood interface. We executed the simulation on HPC systems and analyzed the initiation of blood vessel damage and the propagation of the rupture.

3.3 PD-CVDT model

Our laboratory previously introduced a prototype CVDT model capable of generating the vasculature of the entire human body, approximately 34 billion vessels, and simulating the steady-state hemodynamics [9, 39]. We refer to this prototype model as the Base CVDT model, which serves as the foundation upon which to build supplemental multi-physics models. The generation of the vascular geometry utilized a

Table 2 Simulation parameters for the PeriVessel model.

Parameter	Symbol	Value	Source
Luminal radius	r_0	1.5 mm	[44]
Outer radius	r_1	2 mm	[44]
Vessel length	L	100 mm	This work
Total number of particles	N	54,973	This work
Density	ρ	1.3 g/cm^3	[45]
Elastic modulus	E	3.5 MPa	[46]
Particle spacing	Δx	100 μm	This work
Horizon	δ	350 μm	This work
Critical stretch	s_0	25%	This work
Time step	Δt	500 ns	This work
Total simulation time	t_f	2.25 ms	This work
Net pressure	P_{net}	238 kPa	[31]

recursive fractal algorithm based on the principles of graph theory, following [32, 49]. In this method, the vessels are represented as rigid cylinders connected at junctions. The algorithm created vascular trees starting from a single vessel, in which each vessel bifurcated into two additional vessels. Two symmetric trees were created for each network, representing arterial and venous trees, and the bifurcation process repeated until the trees join at the midplane. An illustrative example network with 30 vessels is shown in Figure 6(a). For each vessel, we created a data structure to store its start and end coordinates, luminal radius, outer radius, length, and indices of connected junctions.

The hemodynamics were based on the Poiseuille equation [50],

$$Q = \frac{\pi r_0^4}{8\eta L}\Delta P, \tag{9}$$

where Q is the blood flow rate in the vessel, r_0 is the vessel's luminal radius, L is the vessel's axial length, η is the blood viscosity, and ΔP is the pressure drop across the vessel. We assembled a system of equations representing the net flow at each vessel junction based on conservation of mass. The blood pressures at each junction were

then solved using iterative linear algebra methods [51], followed by calculation of the flow rate in each vessel using (9).

We coupled the PeriVessel model with the Base CVDT model, together referred to as the PD-CVDT model, to create an integrated CVDT model capable of modeling vascular deformation and damage. We select a vessel in the vascular network, and the vessel data is subsequently shared with the PeriVessel model (Section 3.2) to perform a deformation simulation. An illustrative diagram of the PD-CVDT coupling procedure is shown in Figure 6. The Base CVDT vascular network (Figure 6(a)) determines each vessel's dimensions, blood flow rate, and blood pressure. The Base CVDT model shares the vessel dimensions (i.e., luminal radius, outer radius, and length) and the blood pressure at the vessel endpoints with the PeriVessel model (Figure 6(b)), which then creates a discretized model of the selected vessel and simulates pressure-driven deformation to analyze damage and rupture. To maintain computational efficiency for vessels scaling in length and radius, the PeriVessel model is discretized so that it has the same total number of particles, N, approximately 55,000, regardless of the vessel dimensions. This is accomplished by setting the particle spacing as $\Delta x = (\pi(r_1^2 - r_0^2)L/N)^{1/3}$. The horizon is then selected as $\delta = 3.5\Delta x$. Following Section 3.2, the pressure is applied as a body force density within an artificial boundary layer adjacent to the vessel-blood interface. All other simulation parameters are the same as those of the single vessel model (see Table 2). We performed coupled simulations of vascular networks ranging in size from 33 million to 34 billion vessels to determine the limits of computation feasibility.

3.4 Computational methods and their characteristics

We implemented the algorithms in the C++ programming language using a freely available compiler (the GNU Compiler Collection 12) running on an open-source operating system (Linux, kernel 4.18). We utilized a PD code, CabanaPD (version 0.3),

developed at Oak Ridge National Laboratory [52, 53]. CabanaPD is GPU-enabled, performance-portable, and exascale-capable, and it provides parallel computing functionality through the Message Passing Interface (OpenMPI, version 5.0.5) and Kokkos ecosystem (version 4.5.1) [54]. Although the PeriVessel model is GPU-enabled through CabanaPD, we leave this for future studies and only analyze CPU-based simulations here.

Simulation data was written to a file every 50 time steps using the Hierarchical Data Format (HDF5, version 1.14.3). The output files contained data on each particle's position, displacement, applied forces, strain energy density, and damage. The simulation results were then postprocessed using an open-source data analysis and visualization application (ParaView, version 5.13.0 [55]). Simulations were executed on the Supercomputer Fugaku HPC system at the RIKEN Center for Computational Science [56], the 6^{th} ranked fastest supercomputer at the time of this study (top500.org). At the time of this study, Supercomputer Fugaku contained 158,976 1.8-GHz compute nodes (i.e., CPUs), each with one 48-core processor (ARM A64FX), with a double-precision performance of 2.76 TFLOP/s, 32 GB of shared memory, and an energy efficiency of 54 GFLOP/W.

To determine the computational feasibility of the coupled PD-CVDT model for various vascular network sizes, we followed methods previously described by our laboratory in order to characterize the required computational resources, the complexity, and the scalability of our models [9, 39]. Computational complexity refers to classifying the computational load of an algorithm in terms of its problem size [57]. The problem size, p, represents the input parameter that governs computational resource usage. For instance, the problem size of the Base CVDT model is proportional to the number of vessels in the network, N_V, resulting in a computational complexity of approximately $\mathcal{O}(N_V)$ [9, 39]. The computational complexity can be determined by analyzing the

amount of computational resources required for a given problem size, $R(p)$ [34]. Therefore, we used an open-source profiling tool (Linux perf [58]) to measure the required resources for the PeriVessel model and the coupled PD-CVDT model, and compared the results to those found by previous studies for the Base CVDT model. Specifically, we measured the execution node-time (R_T), the number of FP operations (R_{FP}), and the maximum memory usage (R_M). Node-time is defined as the wall-clock execution time multiplied by the number of compute nodes used. We fit the measured values of each resource to a power-law equation of the form

$$R(p) = \alpha + \beta p^{\gamma}, \tag{10}$$

where α, β, and γ are scalar constants representing the offset, scaling factor, and rate of increase, respectively, for each metric. The Base CVDT and PD-CVDT models scale in proportion to the number of vessels in the vascular network, i.e., $p = N_V$ in (10). However, $N_V = 1$ for the PeriVessel model. We, therefore, characterize the resource usage in the PeriVessel model in terms of the number of compute nodes, i.e., $p = N_c$.

We determined the scalability of the models, which characterizes their ability to utilize additional computing power, typically in the form of supplemental compute nodes [34]. When the problem size is constant while the number of compute nodes increases, it is referred to as strong scaling. We measured strong scaling with the speedup factor,

$$S = \frac{T_w(1)}{T_w(N_c)}, \tag{11}$$

where $T_w(1)$ is the wall-clock time required to execute an algorithm with fixed problem size using a single compute node, and $T_w(N_c)$ is the wall-clock time required to perform the same task using N_c compute nodes. On the other hand, when both the problem size and the number of compute nodes increase proportionally, it is known as weak

scaling [59]. We characterized weak scaling with the parallel efficiency,

$$\varepsilon = \frac{T_w(1,\ p_0)}{T_w(N_c,\ N_c\, p_0)}, \tag{12}$$

where $T_w(1, p_0)$ is the wall-clock time required to execute a task of problem size p_0 using a single compute node, and $T_w(N_c,\ N_c\, p_0)$ is the wall-clock time required to execute a task of problem size $N_c\, p_0$ using N_c compute nodes.

All measurements, for both computational complexity and scalability, were executed while varying the number of compute nodes as $N_c = 2^k$, where $k \in \{0, 1, \ldots, 10\}$. The Base CVDT model and the coupled PD-CVDT model were executed with vascular networks ranging in size from 33 million vessels to 34 billion vessels.

4 Conclusion

In this study, we investigated the feasibility of incorporating biomechanical blood vessel modeling in a cardiovascular digital twin (CVDT) containing the total number of vessels in the average human body. We developed an elastic vessel model based on peridynamics (PD), a non-local theory of solid mechanics, to show blood-pressure-induced damage initiation and propagation, ultimately leading to failure of the vessel wall. The major finding of this study is that, for the first time, modeling blood vessel damage and rupture within a whole-body CVDT was shown to be computationally feasible. Additionally, we ascertained the computational resources required to run these simulations. Notably, we found that the coupled PD-CVDT model, with 34 billion vessels, required a computational cost increase of less than 2% in execution time and memory usage compared to the Base CVDT.

The implication of these findings is that it is possible to include all physiologically-relevant mechanisms needed to model stroke in an entire-body CVDT. Integrating vessel rupture modeling in the Base CVDT necessitated only a modest addition in

terms of computational cost, while providing a significant increase in realism and applicability. A hypothetical use case of this model is for a patient diagnosed with a risk of hemorrhagic stroke. The Base CVDT simulation may be used to identify a vessel of interest, i.e., a vessel with an obstruction, weakened vessel wall, arteriovenous malformation (AVM), or other condition. The PD-CVDT then creates a high-fidelity model of this vessel to determine the probability of rupture as a function of blood pressure, bolstering informed decision-making and preventative measures. Our approach to incrementally add biophysical realism suggests that a fully-realized, general-purpose CVDT model may soon be achievable. Such a capability will open new frontiers in cardiovascular disease research, in which models will include the whole cardiovascular system and all physical phenomena.

At the time this paper was written, few other papers regarding PD simulations of rupture in biological structures were available. We therefore discuss the relation of our work to the few existing studies. PD simulations of rupture in phospholipid biomembranes were performed by Taylor et al. [25], although their method utilized a state-based PD approach based on the linear peridynamic solid (LPS) constitutive material model from [22]. However, the numerical framework and simulation parameters used in their work were similar to those in this study. Both studies considered an elastic constitutive material model and used comparable values for material and simulation parameters. Additionally, Sun et al. [60] developed a fluid-structure interaction model by incorporating Fung's hyperelastic material model into bond-based PD to simulate aneurysm rupture in vessels. While this model showed good accuracy in modeling single, isolated blood vessels, there has been no work to show vessel rupture or damage in a multi-vessel network. Computationally, we found the complexity and scalability of the models to be similar to those reported by previous studies from our laboratory [9, 39, 61].

A major strength of this study is the focus on the computational aspects of the PeriVessel model. We performed extensive analyses of resource use, computational complexity, and scalability to characterize the tradeoffs between simulation fidelity and computational cost. This information is critical for the future of CVDT research, as striking a judicious balance between realism and efficiency is paramount when scaling vessel mechanics simulations to include the entire vasculature of the human body. A possible limitation of this study is the choice of constitutive material model for the blood vessel. Studies such as those by Fung et al. [62] have found that the vessel wall typically behaves mechanically as a hyperelastic material. We used the PMB constitutive material model because it is computationally more efficient than the LPS model. However, the elastic response of the PMB model is restricted to a Poisson's ratio of $\nu = 1/4$ in 3D [35], which limits the underlying hyperelastic behavior. Nevertheless, we do not consider this a significant limitation because CabanaPD already implements the LPS model, which removes the restriction on Poisson's ratio; therefore, this study could be readily extended to use the LPS model. Note that the goal of this study was to assess computational feasibility rather than to model rupture with maximal physiological accuracy. Additionally, in this study, we only considered deformation due to pressure on the vessel wall. However, vasodilation and other biophysical mechanisms may influence the deformation of a vessel wall due to changes in the mechanical properties of the wall. Our laboratory is currently working on modeling nitric-oxide-mediated vasodilation in vascular frameworks.

Although we utilized some biological simplifications, this work achieved promising results and provides a general strategy and computational benchmark for modeling vessel rupture within a whole-body CVDT. Future improvements to the model must be made in order to achieve a clinically-applicable model, such as using a more sophisticated, state-based PD constitutive material model. Future work in this area may

involve implemented GPU-based calculations through CabanaPD and probing the possible computational performance boosts, as mentioned in Section 3.4. Additionally, more work must be done to improve the predictive capabilities of the models. It is not feasible to model all vessels of the human body with PD. It would be, therefore, necessary to use a heuristic model or an artificial intelligence algorithm, implemented with the Base CVDT model, to identify at-risk vessels to be modeled by the PeriVessel model. Although this study demonstrated coupling of our prototype Base CVDT with a biomechanical deformation model, a fully-realized CVDT must include integration of multiple models of biophysics to analyze the relationships involved in physiological processes.

Declarations

Funding. M. Cole and W. Newhauser were supported by the Bella Bowman Foundation. This work used computational resources of the Supercomputer Fugaku provided by RIKEN through the HPCI System Research Project (Project ID: ra250021) with P. Diehl as PI. P. Seleson was supported by the Laboratory Directed Research and Development Program of Oak Ridge National Laboratory, managed by UT-Battelle, LLC, for the U. S. Department of Energy. P. Diehl was supported by the U.S. Department of Energy through the Los Alamos National Laboratory. Los Alamos National Laboratory is operated by Triad National Security, LLC, for the National Nuclear Security Administration of U.S. Department of Energy (Contract No. 89233218CNA000001). Approved by Los Alamos National Laboratory as LA-UR-25-30541.

Competing interests. The authors declare that they have no financial or non-financial interests that could be perceived as influencing this work.

Ethics approval and consent to participate. Not applicable

Consent for publication. Not applicable

Data availability. Not applicable

Materials availability. Not applicable

Code availability. The source code is not publicly available at this time. Researchers interested in using the code or pursuing collaboration are encouraged to contact the authors.

Author contribution. MC carried out the modeling and developed the computational code. PD, WN, and PS supervised the modeling and code development. WN provided funding to support MC's work as a PhD student. All authors contributed to writing and revising the manuscript.

References

[1] Shang, Y.: Localized recovery of complex networks against failure. Scientific Reports **6**(1), 30521 (2016)

[2] Di Cesare, M., Perel, P., Taylor, S., Kabudula, C., Bixby, H., Gaziano, T.A., McGhie, D.V., Mwangi, J., Pervan, B., Narula, J., *et al.*: The heart of the world. Global Heart **19**(1), 11 (2024)

[3] Penn, D.L., Komotar, R.J., Connolly, E.S.: Hemodynamic mechanisms underlying cerebral aneurysm pathogenesis. Journal of Clinical Neuroscience **18**(11), 1435–1438 (2011)

[4] Rice-Canetto, T.E., Ueno, A., Whitney, E., Reier, L., Houston, R., Siddiqi, J.: A review of the current literature on cerebral aneurysms. Cureus **17**(3) (2025)

[5] Sánchez-Molina, D., García-Vilana, S., Llumà, J., Galtés, I., Velázquez-Ameijide, J., Rebollo-Soria, M.C., Arregui-Dalmases, C.: Mechanical behavior of blood vessels: elastic and viscoelastic contributions. Biology **10**(9), 831 (2021)

[6] Hademenos, G.J.: The physics of cerebral aneurysms. Physics Today **48**(2), 24–30 (1995)

[7] Caro, C.G., Pedley, T.J., Schroter, R.C., Seed, W.A., Parker, K.H.: The Mechanics of the Circulation, 2nd edn. Cambridge University Press, Cambridge, UK (2012)

[8] Corral-Acero, J., Margara, F., Marciniak, M., Rodero, C., Loncaric, F., Feng, Y., Gilbert, A., Fernandes, J.F., Bukhari, H.A., Wajdan, A., *et al.*: The 'Digital Twin' to enable the vision of precision cardiology. European Heart Journal **41**(48), 4556–4564 (2020)

[9] Newhauser, W., Cole, M., Diehl, P., Moreno, J., Kaiser, H., Tohid, R., Nader, N., Chancellor, J.: Toward a cardiovascular digital twin: Modeling the entire human vasculature using supercomputing. Submitted (2026)

[10] Lejeune, E., Linder, C.: Modeling biological materials with peridynamics. In: Oterkus, E., Oterkus, S., Madenci, E. (eds.) Peridynamic Modeling, Numerical Techniques, and Applications. Elsevier Series in Mechanics of Advanced Materials, pp. 249–273. Elsevier, Oxford (2021)

[11] Vito, R.P., Dixon, S.A.: Blood vessel constitutive models—1995–2002. Annual Review of Biomedical Engineering **5**(1), 413–439 (2003)

[12] Lai, W.M., Rubin, D., Krempl, E.: Introduction to Continuum Mechanics, 4th edn. Butterworth-Heinemann, Cambridge (2010)

[13] Reddy, J.N.: Introduction to the Finite Element Method, 3rd edn. McGraw-Hill Education, New York (2006)

[14] Raghavan, M.L., Vorp, D.A.: Toward a biomechanical tool to evaluate rupture

potential of abdominal aortic aneurysm: identification of a finite strain constitutive model and evaluation of its applicability. Journal of Biomechanics **33**(4), 475–482 (2000)

[15] Seshaiyer, P., Humphrey, J.D.: On the potentially protective role of contact constraints on saccular aneurysms. Journal of Biomechanics **34**(5), 607–612 (2001)

[16] Silling, S.A.: Reformulation of elasticity theory for discontinuities and long-range forces. Journal of the Mechanics and Physics of Solids **48**(1), 175–209 (2000)

[17] Javili, A., Morasata, R., Oterkus, E., Oterkus, S.: Peridynamics review. Mathematics and Mechanics of Solids **24**(11), 3714–3739 (2019)

[18] Gdoutos, E.E.: Fracture Mechanics: An Introduction, 3rd edn. Solid Mechanics and Its Applications, vol. 263. Springer, Cham (2020)

[19] Song, J.-H., Wang, H., Belytschko, T.: A comparative study on finite element methods for dynamic fracture. Computational Mechanics **42**(2), 239–250 (2008)

[20] Moës, N., Dolbow, J., Belytschko, T.: A finite element method for crack growth without remeshing. International Journal for Numerical Methods in Engineering **46**(1), 131–150 (1999)

[21] Belytschko, T., Liu, W.K., Moran, B., Elkhodary, K.: Nonlinear Finite Elements for Continua and Structures, 2nd edn. John Wiley & Sons, Chichester (2014)

[22] Silling, S.A., Epton, M., Weckner, O., Xu, J., Askari, E.: Peridynamic states and constitutive modeling. Journal of Elasticity **88**(2), 151–184 (2007)

[23] Dahal, B., Seleson, P., Trageser, J.: The evolution of the peridynamics co-authorship network. Journal of Peridynamics and Nonlocal Modeling **5**(3),

311–355 (2023)

[24] Deng, Q., Chen, Y., Lee, J.D.: An investigation of the microscopic mechanism of fracture and healing processes in cortical bone. International Journal of Damage Mechanics **18**(5), 491–502 (2008)

[25] Taylor, M., Gözen, I., Patel, S., Jesorka, A., Bertoldi, K.: Peridynamic modeling of ruptures in biomembranes. PloS ONE **11**(11) (2016) https://doi.org/10.1371/journal.pone.0165947 e0165947

[26] Lejeune, E., Linder, C.: Modeling tumor growth with peridynamics. Biomechanics and Modeling in Mechanobiology **16**(4), 1141–1157 (2017)

[27] Lejeune, E., Linder, C.: Interpreting stochastic agent-based models of cell death. Computer Methods in Applied Mechanics and Engineering **360**, 112700 (2020)

[28] Diehl, P., Lipton, R., Wick, T., Tyagi, M.: A comparative review of peridynamics and phase-field models for engineering fracture mechanics. Computational Mechanics **69**(6), 1259–1293 (2022)

[29] Dorduncu, M., Ren, H., Zhuang, X., Silling, S., Madenci, E., Rabczuk, T.: A review of peridynamic theory and nonlocal operators along with their computer implementations. Computers & Structures **299**, 107395 (2024)

[30] Wang, X., Wang, Q., An, B., He, Q., Wang, P., Wu, J.: A GPU parallel scheme for accelerating 2D and 3D peridynamics models. Theoretical and Applied Fracture Mechanics **121**, 103458 (2022)

[31] Ciszek, B., Cieślicki, K., Krajewski, P., Piechnik, S.K.: Critical pressure for arterial wall rupture in major human cerebral arteries. Stroke **44**(11), 3226–3228 (2013)

[32] Donahue, W.P., Newhauser, W.D.: Computational feasibility of simulating whole-organ vascular networks. Biomedical Physics & Engineering Express **6**(5), 055028 (2020)

[33] Amdahl, G.M.: Validity of the single processor approach to achieving large scale computing capabilities. In: Proceedings of the April 18-20, 1967, Spring Joint Computer Conference, Atlantic City, NJ, pp. 483–485 (1967)

[34] Shoukourian, H., Wilde, T., Auweter, A., Bode, A.: Predicting the energy and power consumption of strong and weak scaling HPC applications. Supercomputing Frontiers and Innovations: an International Journal **1**(2), 20–41 (2014)

[35] Silling, S.A., Askari, E.: A meshfree method based on the peridynamic model of solid mechanics. Computers & Structures **83**(17-18), 1526–1535 (2005)

[36] Seleson, P., Parks, M.L., Gunzburger, M., Lehoucq, R.B.: Peridynamics as an upscaling of molecular dynamics. Multiscale Modeling & Simulation **8**(1), 204–227 (2009)

[37] Seleson, P., Parks, M.L., Gunzburger, M.: Peridynamic state-based models and the embedded-atom model. Communications in Computational Physics **15**(1), 179–205 (2014)

[38] Madenci, E., Oterkus, E.: Peridynamic Theory and Its Applications. Springer, New York, NY (2013)

[39] Cole, M., Newhauser, W., Diehl, P., Domke, J.: Petascale simulations of the whole human cardiovascular system including pulsatile blood flow. In Preparation (2026)

[40] Behera, D., Roy, P., Anicode, S.V.K., Madenci, E., Spencer, B.: Imposition of local boundary conditions in peridynamics without a fictitious layer and unphysical stress concentrations. Computer Methods in Applied Mechanics and Engineering **393**, 114734 (2022)

[41] Macek, R.W., Silling, S.A.: Peridynamics via finite element analysis. Finite Elements in Analysis and Design **43**(15), 1169–1178 (2007)

[42] Lipton, R.P., Jha, P.K.: Nonlocal elastodynamics and fracture. Nonlinear Differential Equations and Applications NoDEA **28**(3), 23 (2021)

[43] Birner, M., Diehl, P., Lipton, R., Schweitzer, M.A.: A fracture multiscale model for peridynamic enrichment within the partition of unity method. Advances in Engineering Software **176**, 103360 (2023)

[44] Mandell, D.M., Mossa-Basha, M., Qiao, Y., Hess, C.P., Hui, F., Matouk, C., Johnson, M.H., Daemen, M.J.A.P., Vossough, A., Edjlali, M., *et al.*: Intracranial Vessel Wall MRI: Principles and Expert Consensus Recommendations of the American Society of Neuroradiology. American Journal of Neuroradiology **38**(2), 218–229 (2017)

[45] Jahangiri, M., Saghafian, M., Sadeghi, M.R.: Numerical simulation of hemodynamic parameters of turbulent and pulsatile blood flow in flexible artery with single and double stenoses. Journal of Mechanical Science and Technology **29**(8), 3549–3560 (2015)

[46] Ebrahimi, A.P.: Mechanical properties of normal and diseased cerebrovascular system. Journal of Vascular and Interventional Neurology **2**(2), 155–162 (2009)

[47] Bobaru, F., Ha, Y.D.: Adaptive refinement and multiscale modeling in 2D peridynamics. International Journal for Multiscale Computational Engineering **9**(6),

635–659 (2011)

[48] Verlet, L.: Computer "Experiments" on Classical Fluids. I. Thermodynamical Properties of Lennard-Jones Molecules. Physical Review **159**(1), 98 (1967)

[49] Olufsen, M.S.: Structured tree outflow condition for blood flow in larger systemic arteries. American Journal of Physiology-Heart and Circulatory Physiology **276**(1), 257–268 (1999)

[50] Sutera, S.P., Skalak, R.: The history of Poiseuille's law. Annual Review of Fluid Mechanics **25**(1), 1–19 (1993)

[51] Van der Vorst, H.A.: Iterative Krylov Methods for Large Linear Systems vol. 13. Cambridge University Press, Cambridge (2003)

[52] Reeve, S., Seleson, P., Diehl, P.: CabanaPD. https://doi.org/10.5281/zenodo.13844547

[53] Reeve, S.T., Fattebert, J.-L., DeWitt, S., Seleson, P., Joy, D., Slattery, S., Scheinberg, A., Halver, R., Junghans, C., Negre, C.F., *et al.*: Co-design for Particle Applications at Exascale. Computing in Science & Engineering **26**(2), 43–52 (2024)

[54] Trott, C.R., Lebrun-Grandié, D., Arndt, D., Ciesko, J., Dang, V., Ellingwood, N., Gayatri, R., Harvey, E., Hollman, D.S., Ibanez, D., Liber, N., Madsen, J., Miles, J., Poliakoff, D., Powell, A., Rajamanickam, S., Simberg, M., Sunderland, D., Turcksin, B., Wilke, J.: Kokkos 3: Programming model extensions for the exascale era. IEEE Transactions on Parallel and Distributed Systems **33**(4), 805–817 (2022)

[55] Ahrens, J., Geveci, B., Law, C.: ParaView: An End-User Tool for Large Data

Visualization. Visualization Handbook **717**(8) (2005)

[56] Shimizu, T.: Supercomputer Fugaku: Co-designed with application developers/researchers. In: 2020 IEEE Asian Solid-State Circuits Conference (A-SSCC), 9-11 November 2020, Hiroshima, Japan, pp. 1–4 (2020)

[57] Van Tilborg, H.C., Jajodia, S.: Encyclopedia of Cryptography and Security. Springer, New York (2014)

[58] Domingos, J.M., Rocha, T., Neves, N., Roma, N., Tomás, P., Sousa, L.: Supporting RISC-V Performance Counters Through Linux Performance Analysis Tools. In: 2023 IEEE 34th International Conference on Application-Specific Systems, Architectures and Processors (ASAP), pp. 94–101 (2023)

[59] Hamann, H., Reina, A.: Scalability in computing and robotics. IEEE Transactions on Computers **71**(6), 1453–1465 (2021)

[60] Sun, W.-K., Yin, B., Zhang, L.-W., Liew, K.: Blood pressure-driven rupture of blood vessels. Journal of the Mechanics and Physics of Solids **174**, 105–274 (2023)

[61] Cole, M., Newhauser, W., Diehl, P.: Simulating vasodilation in the entire human body. In Preparation (2026)

[62] Fung, Y., Fronek, K., Patitucci, P.: Pseudoelasticity of arteries and the choice of its mathematical expression. American Journal of Physiology-Heart and Circulatory Physiology **237**(5), 620–631 (1979)

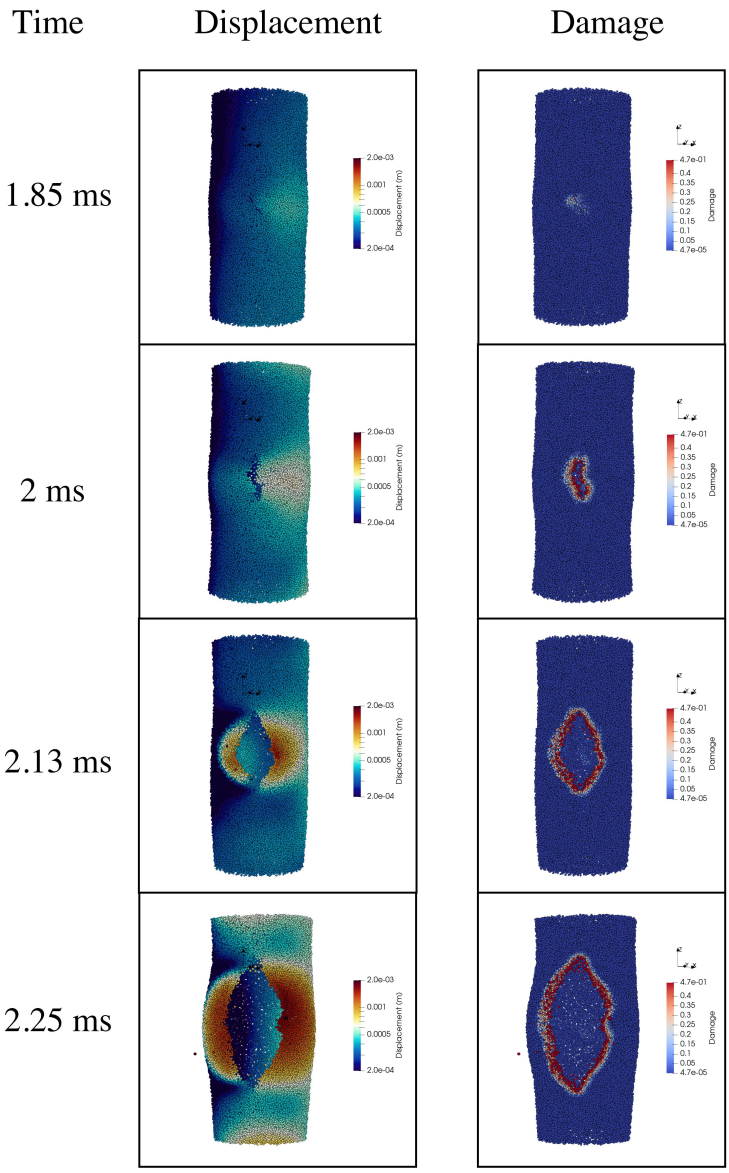

Fig. 1 PeriVessel rupture simulation at four time points. The left column displays computational particles with colors representing the magnitude of their displacement, and the right column depicts the same particles with colors representing their damage.

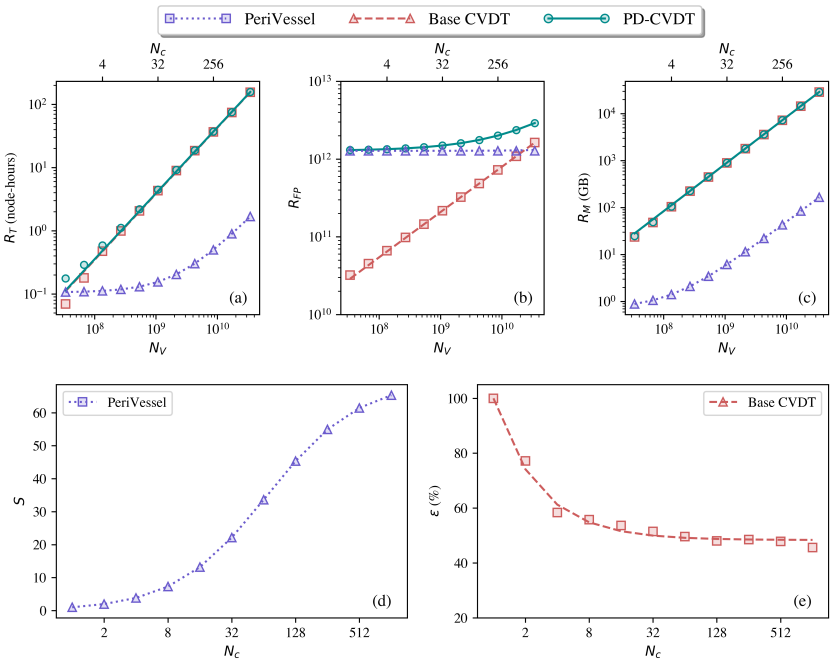

Fig. 2 Computational resource usage and scalability of the models, including (a) node time, T; (b) floating point, FP, operations; (c) maximum memory, M; (d) speedup factor, S; and (e) parallel efficiency, ε. The markers represent measured values, while the lines show the empirical fit to (10). Results are shown for the PeriVessel model in purple, for the Base CVDT model in red, and for the coupled PD-CVDT model in green. In (a)-(c), the bottom x-axis is the number of vessels, N_V, while the top x-axis shows the number of compute nodes used, N_c. The resource usage of the Base CVDT model and the coupled PD-CVDT model were directly proportional to N_V. However, the PeriVessel model only ever includes one vessel, and thus has no relation to N_V. Therefore, the resource usage of the PeriVessel model is shown in proportion to the number of compute nodes used, N_c. The strong scalability of the PeriVessel model is seen in (d), which plots S versus N_c, while the weak scalability of the Base CVDT model is seen in (e), which plots ε versus N_c.

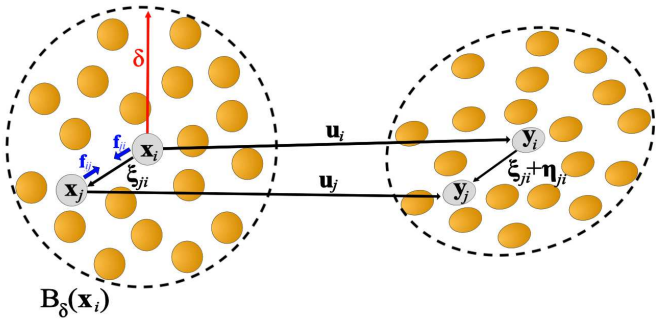

Fig. 3 Illustration showing the peridynamic formulation highlighting two particles, i and j, within an elastic body undergoing deformation. The dashed line represents the neighborhood of i, $B_\delta(\mathbf{x}_i)$, with the horizon, δ, denoted by the red arrow. On the left is the reference (undeformed) configuration, in which the particles are represented by the yellow circles. The particle at $\mathbf{x}_i$ interacts with the particle at $\mathbf{x}_j$ through the bond $\boldsymbol{\xi}_{ji}$. On the right is the body in the deformed configuration, where the bond between the particles, now at their deformed positions $\mathbf{y}_i$ and $\mathbf{y}_j$, is stretched and has become $\boldsymbol{\xi}_{ji} + \boldsymbol{\eta}_{ji}$, where $\boldsymbol{\eta}_{ji}$ is their relative displacement. The blue arrows represent intrinsic bond force densities acting between the particles, where $\mathbf{f}_{ji}$ is the force density from particle j acting on particle i, and $\mathbf{f}_{ij}$ is the force density from particle i acting on particle j.

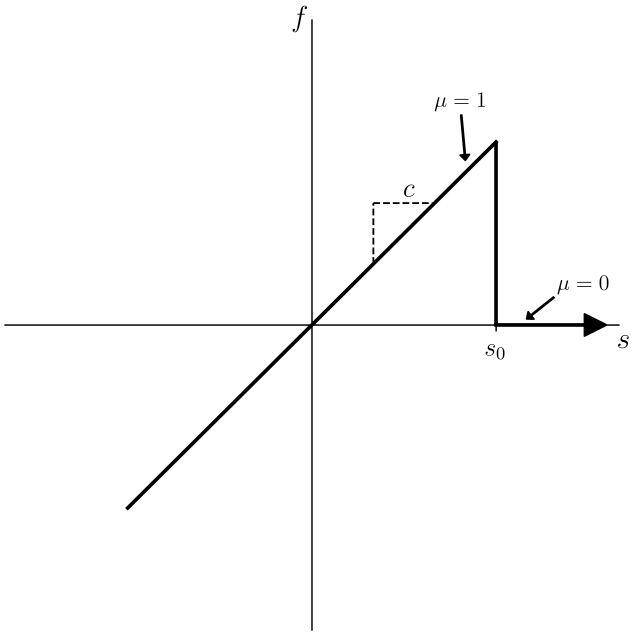

Fig. 4 Illustration of the relationship between the magnitude of the bond force density, f, and the bond stretch, s, in the PMB constitutive material model described by Silling and Askari [35]. The slope of the graph in the elastic regime is the bond elastic constant, c, from (2). The bond force density increases as the bond stretch increases, while the bond is intact ($\mu = 1$), until it reaches the critical stretch, s_0, at which point the bond breaks ($\mu = 0$) and the bond force density goes to zero.

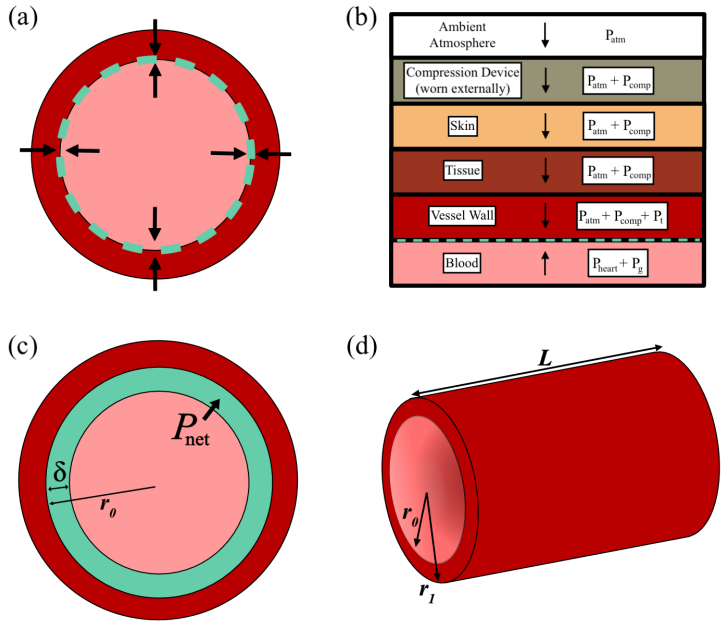

Fig. 5 PeriVessel model and acting pressures (figures not to scale). (a) Axial view of the PeriVessel model with arrows showing the forces applied at the vessel-blood interface, denoted by the green dashed line. (b) Illustrative diagram of pressures acting on the vessel-blood interface from (7). (c) Axial view of the PeriVessel model showing the net pressure, P_{net}, applied to the boundary layer, represented by the green region with thickness δ. (d) Illustration of the vessel geometry used in the PD simulation.

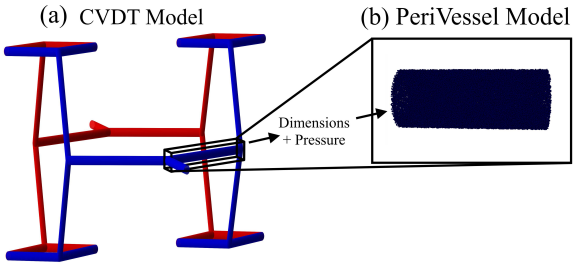

Fig. 6 Illustrative example of the coupled PD-CVDT model. (a) Vascular network with 30 vessels from the Base CVDT model. The red cylinders represent arteries and the blue cylinders represent veins. (b) Depiction of the PeriVessel model, simulating a single vessel of interest from the Base CVDT model.